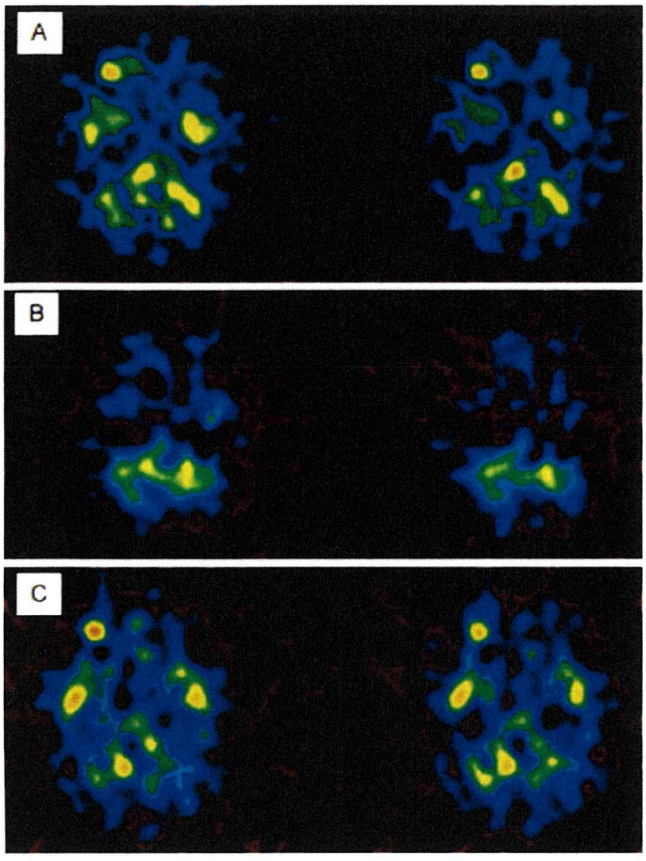

Figure 6. A Pretherapeutic I-123 IMP SPECT delayed images of a 61-year-old woman with malignant melanoma. The lesion shows obvious accumulation. The retention index was 70.7, and the T/N ratio was 2.1. **B** Post-therapeutic examination performed 6 months after transpupillary thermotherapy (TTT) shows an insufficient decrease of the uptake. The retention index was 63.0, and the T/N ratio was 1.6. **C** A follow-up examination performed 2 years after TTT showed a relapse of the tumor. The retention index was 92.7, and the T/N ratio was 2.3. Applying the ROI template makes the semiquantification more reliable, especially when the same lesions are examined repeatedly.

lesions, on the other hand, tend to be underestimated in relation to the protruded tumor. For example, the T/N ratio of a ciliary body melanocytoma was 1.2, which is the upper limit for a nonmelanoma lesion, but the retention index was 19.1, which was low. In another case of malignant melanoma, the retention index was 783.3, which is extremely high. These figures depend on the nontumoral side count of the early phase. Because the high accumulated noise of the early phase sometimes causes a high retention index, the standard deviation of the retention index is also high. For these reasons, the two parameters should be considered to be complementary. In this study, four of the six cases that turned out to be false negatives by the retention index were diagnosed correctly by the T/N ratio. On the other hand, only one of the three cases which were false negatives by the T/N ratio was diagnosed correctly by the retention index. The positive predictive value of the T/N ratio was better than that of the retention index. Two of the six cases that were false positives with the T/N ratio were diagnosed correctly by the retention index. Both were hemangiomas. The other four cases were false positives by the retention index, too. They consisted of two melanocytomas, a nevocellular nevus, and a post-therapeutic malignant melanoma. The negative predictive value of the retention index was better than that of the T/N ratio.

Another factor leading to inaccuracy in this study is the possibility of incomplete standardization. Two cases were possibly the result of incomplete standardization. One was a malignant melanoma that showed false negative results with both the retention index and the T/N ratio, despite an obvious accumulation on SPECT imaging. In cases of severe atrophy or deformity of the brain cortex, incomplete standardization might occur. Moreover, when the distance between the orbit and the bottom of the frontal lobe is greater than average, false negative results might occur, and when the distance is shorter, false positive results might occur.

In conclusion, new semiquantitative estimation of malignant melanoma using an original 3D-template and standardized I-123 IMP scintigraphy was assessed. The accuracy was 83.6% by the retention index, and 85.2% by the T/N ratio. This method is considered to be reproducible and objective, and it is more useful when the examinations are performed repeatedly for the estimation of the therapy and follow-up.

Acknowledgments. The authors are indebted to Prof. J. Patrick Barron of the International Medical Communications Center of Tokyo Medical University for his review of this manuscript.

References

1. Sou R, Oku N, Ohguro N, Hibino S, Fujikado T, Tano Y. The clinical role of *N*-isopropyl-*p*-[^{123}I]-iodoamphetamine single photon emission computed tomography in the follow-up of choroidal melanoma after radiotherapy. Jpn J Ophthalmol 2004;48:54–58.
2. Morimoto K, Yoshimura M, Goto H, Koizumi K, Abe K. Semiquantitative evaluation of uveal malignant melanoma with *N*-isopropyl-*p*-[^{123}I]-iodoamphetamine (I-123 IMP). J Tokyo Med Univ 2007;65:137–143.
3. Goto H. Clinical efficacy of I-123 IMP SPECT for the diagnosis of malignant uveal melanoma. Int J Clin Oncol 2004;9:74–78.
4. Kotake F, Kawanishi M, Ishii I, Akata S, Kakizaki D, Abe K. A case of choroidal malignant melanoma in which I-123 IMP scintigraphy was useful for diagnosis. Kaku Igaku 1998;35:427–433.
5. Minoshima S, Koeppe RA, Frey KA, Kuhl DE. Anatomic standardization: linear scaling and nonlinear warping of functional brain images. J Nucl Med 1994;35:1528–1537.
6. Minoshima S, Koeppe RA, Mintun MA, et al. Automated detection of the intercommissural line for stereotactic localization of functional brain images. J Nucl Med 1993;34:322–329.
7. Prichard RS, Hill AD, Skehan SJ, O'Higgins N. Positron emission tomography for staging and management of malignant melanoma. Br J Surg 2002;89:389–396.
8. Kato K, Kubota T, Ikeda M, et al. Low efficacy of ^{18}F-FDG PET for detection of uveal malignant melanoma compared with ^{123}I-IMP SPECT. J Nucl Med 2006;47:404–409.

9. Murata K, Suzuki K, Ayakawa Y, Higashi N, Lin PP. Comparison of I-123 IMP and Ga-67 citrate scintigraphy of malignant melanoma. Clin Nucl Med 2003;28:704–708.
10. Watanabe M, Seto H, Yokoyama K, et al. Scintigraphic study of malignant melanoma with I-123 iodoamphetamine. Nucl Med Commun 1996;17:153–159.
11. Satoh M, Ishikawa N, Takeda T, et al. Clinical assessment of I-123 IMP scintigraphy in malignant melanoma. Jpn J Clin Radiol 1991;36:913–918.

INCREASES OF VITREOUS MONOCYTE CHEMOTACTIC PROTEIN 1 AND INTERLEUKIN 8 LEVELS IN PATIENTS WITH CONCURRENT HYPERTENSION AND DIABETIC RETINOPATHY

YOSHIHIRO WAKABAYASHI, MD,* YOSHIHIKO USUI, MD,* YOKO OKUNUKI, MD,† TAKESHI KEZUKA, MD,* MASARU TAKEUCHI, MD,* TAKUYA IWASAKI, MD,* ATSUSHI OHNO, MD,‡ HIROSHI GOTO, MD*

Purpose: To investigate whether concurrent hypertension affects vitreous cytokine levels in diabetic retinopathy.

Methods: Vitreous samples from 41 patients with diabetic retinopathy with or without concurrent hypertension, who underwent vitrectomy, were collected. Vitreous cytokine concentrations were simultaneously measured using flow cytometry. Patients were stratified according to hypertension or other clinical conditions, and the differences in vitreous levels of monocyte chemotactic protein 1, interleukin 8, vascular endothelial growth factor, interferon-inducible protein 10, and monokine induced by interferon gamma were examined.

Results: Vitreous levels of monocyte chemotactic protein 1 and interleukin 8 were significantly ($P < 0.05$) higher in hypertensive patients than in nonhypertensive patients and were significantly ($P < 0.05$) higher in active diabetic retinopathy than in inactive diabetic retinopathy. Vitreous levels of vascular endothelial growth factor, interferon-inducible protein 10, and monokine induced by interferon gamma were not affected by the coexistence of hypertension. In multivariate models, active diabetic retinopathy ($P = 0.004$ and $P = 0.007$), systolic blood pressure ($P = 0.039$ and $P = 0.041$), and hypertension ($P = 0.032$ and $P = 0.035$) were significant and independent predictors for increased vitreous monocyte chemotactic protein 1 and interleukin 8 levels.

Conclusion: Both monocyte chemotactic protein 1 and interleukin 8 levels were elevated in the vitreous of patients with diabetic retinopathy and concurrent hypertension. These findings may help to explain the epidemiologic and clinical evidence that systemic hypertension exacerbates diabetic retinopathy.

RETINA 31:1951–1957, 2011

Diabetic retinopathy is a major cause of vision loss in many countries.[1] Although the pathogenesis of diabetic retinopathy is not fully understood, the onset and progression are mediated by chronic inflammatory processes.[2] In diabetic retinopathy, leukocytes infiltrate the retina.[3,4] Chemokines are a family of structurally related cytokines involved in the activation and directed migration of leukocytic cells that mediate inflammation.[5,6] A number of chemokines are detected in the vitreous of patients with diabetic retinopathy.[7,8] Thus, it is possible that chemokines in the vitreous promote leukocyte migration and adhesion to vascular endothelial cells, resulting in increased vascular permeability and neovascularization, and thereby to the onset and progression of diabetic retinopathy.[9,10]

Systemic hypertension and proteinuria have been clearly identified in epidemiologic studies as independent risk factors for diabetic retinopathy.[11,12] Clinically, high blood pressure and renal dysfunction have detrimental effects on diabetic retinopathy, but the mechanisms underlying the effects of these systemic factors on the pathogenesis of diabetic retinopathy are not clear.

Chemokines, including monocyte chemotactic protein 1 (MCP-1)[13] and interleukin 8 (IL-8), are present

in the vascular lesions of hypertensive rats.[14] These chemokines are associated with vascular inflammatory responses induced by hypertension and the development of vascular remodeling, including atherosclerosis. Recently, we performed a prospective case–control study to measure a panel of chemokines in the vitreous samples from patients with diabetic retinopathy and found that vitreous levels of vascular endothelial growth factor (VEGF), interferon gamma–inducible protein 10 (IP-10), monokine induced by interferon gamma (Mig), MCP-1, and IL-8 were elevated in patients with diabetic retinopathy.[15] There are few reports, however, on the relationship between intraocular chemokines and systemic risk factors, especially hypertension, in diabetic retinopathy. In the present study, we performed a subgroup analysis of the data from the prospective case–control study to investigate whether clinical risk factors, including concurrent hypertension, affect the vitreous levels of VEGF, IP-10, Mig, MCP-1, and IL-8 that were found by our previous study to be elevated in diabetic retinopathy.

Subjects and Methods

Patients

Forty-one eyes of 41 consecutive patients with diabetic retinopathy who underwent pars plana vitrectomy by standard 3-port incisions at the Hachiouji Medical Center of Tokyo Medical University were included in the study. Twenty-four eyes underwent vitrectomy because of vitreous hemorrhage or traction retinal detachment, and 17 eyes underwent the surgery because of macular edema. The study was approved by the institutional review committee of the Tokyo Medical University. Informed consent for surgery and vitreous sampling was obtained from all subjects. Exclusion criteria for this study were 1) previous ocular surgery and 2) a history of ocular inflammation and other vitreoretinal diseases.

The patients, all with diabetic retinopathy (25 men, 16 women), were Japanese and had a median age of 63 years (range, 27–78 years). The mean hemoglobin A_{1C} level was 6.7% (range, 5.0–12.0%), and the mean duration of diabetes was 14.4 years (range, 6.1–28.2 years). Four patients had Type 1 diabetes, and 37 patients had Type 2 diabetes. Twenty-four patients had concurrent hypertension and were being treated with antihypertensive agents. Sixteen patients were receiving treatment for concurrent hyperlipidemia.

Hypertension and hyperlipidemia were diagnosed and treated by the physician (A.O.) with expert knowledge about diabetes mellitus. The systolic and diastolic blood pressures used in the analyses were the averages of the last two of three measurements according to the protocol of the Hypertension Detection and Follow-up Program.[16] A diagnosis of hypertension necessitating oral antihypertensive agents was defined as a mean systolic blood pressure of $\geq$140 mmHg, or a mean diastolic blood pressure of $\geq$90 mmHg, according to the Japanese guideline for the management of hypertension.[17] Among the 24 hypertensive patients, 21 (88%) were treated with Angiotensin II receptor blockers (ARB), 15 (63%) with calcium channel blockers, and 10 (42%) with other antihypertensive agents. Fourteen patients (58%) were treated with >2 kinds of antihypertensive agents. Blood pressure control aimed at a systolic blood pressure of <130 mmHg and a diastolic blood pressure <80 mmHg.[17] Clinical characteristics including age, sex, diabetes type, and insulin use of the enrolled patients were obtained from the medical records. Systolic and diastolic blood pressures used in the statistical analysis were measured in the early morning on the day of ocular surgery. Fasting serum total cholesterol, serum creatinine, hemoglobin A_{1C}, and urinalysis data were obtained within the 2 weeks before surgery.

Fundus Findings

Slit-lamp microscopic examination using a fundus contact lens or fluorescein angiography was used for diagnosis. When the fundus examination findings were obscure because of preoperative vitreous hemorrhage, the diagnosis was made based on intraoperative findings. Patients were classified into 2 groups, active diabetic retinopathy (30 eyes) and inactive diabetic retinopathy (11 eyes). Active diabetic retinopathy was defined as eyes with proliferative diabetic retinopathy showing patent new vessels in the retina or optic disk.[8] Inactive diabetic retinopathy was defined as eyes with nonproliferative diabetic retinopathy and quiescent proliferative diabetic retinopathy showing no patent new vessels. Thirty-seven eyes were treated with pan retinal photocoagulation before surgery.

From the *Department of Ophthalmology and Departments of †Ophthalmology and ‡Diabetology, Endocrinology and Metabolism, Hachiouji Medical Center, Tokyo Medical University, Tokyo, Japan.

Y. Wakabayashi, Y. Usui, and Y. Okunuki contributed equally to this study.

The authors have no financial interest or conflicts of interest.

Reprint requests: Yoshihiro Wakabayashi, MD, Department of Ophthalmology, Tokyo Medical University, 6-7-1, Nishishinjuku, Shinjuku-ku, Tokyo, 160-0023, Japan; e-mail: wbaki@tokyo-med.ac.jp

Vitreous Sample Collection and Measurements of Cytokines

Vitreous samples, 0.1 mL to 0.5 mL, were removed from the midvitreous with a vitreous cutter at the start of vitrectomy before intraocular infusion. The vitreous samples were collected into sterile tubes and stored immediately at −80°C until assay. The samples were assayed within 6 months after collection. Vitreous samples were assessed for cytokines including human VEGF, IP-10, Mig, MCP-1, and IL-8 using the Cytometric Bead Array Flex immunoassay kit (PharMingen, San Diego, CA), as described previously.[15,18] The lowest detectable concentration of this assay was 1.0 pg/mL for all cytokines tested.

Statistical Analysis

Vitreous concentrations of cytokines and all clinical data are expressed as median (range). To evaluate the association of the vitreous VEGF, IP-10, Mig, MCP-1, and IL-8 concentrations with various clinical factors, patients were divided into 2 groups according to the presence or absence of insulin use, hypertension, hyperlipidemia, proteinuria, active diabetic retinopathy, and antihypertensive agent treatment. A Wilcoxon rank sum test was used to compare vitreous cytokine concentrations between the two groups. Spearman rank correlation test was used to examine correlations of vitreous MCP-1 and IL-8 concentrations with age, hemoglobin A_{1C}, systolic and diastolic blood pressures, and serum total cholesterol and creatinine. Data with a skewed distribution were transformed to a logarithmic scale, and stepwise multiple regression analysis was performed to select the independent clinical factors related to the vitreous levels of MCP-1 and IL-8. A P value of <0.05 was considered statistically significant. All analyses were performed using JMP statistical analysis software, Version 5.01J (SAS Institute, Cary, NC).

Results

The median (range) vitreous concentrations of MCP-1, IL-8, VEGF, IP-10, and Mig in all subjects were 1,200.5 pg/mL (35.6–7,823.3 pg/mL), 31.8 pg/mL (1.0–314.3 pg/mL), 376.3 pg/mL (21.0–2,877.0 pg/mL), 295.6 pg/mL (33.3–1,000.3 pg/mL), and 199.7 pg/mL (20.6–997.2 pg/mL), respectively. Vitreous MCP-1 concentrations were significantly higher in hypertensive patients than in nonhypertensive patients (1,597.7 pg/mL [284.3–7,823.3 pg/mL] vs. 865.5 pg/mL [35.6–5,780.5 pg/mL], $P < 0.05$; Table 1). Vitreous MCP-1 concentrations were significantly higher in patients with active diabetic retinopathy than in those with inactive diabetic retinopathy (1,428.7 pg/mL [456.4–7,823.3 pg/mL] vs. 614.3 pg/mL [35.6–2,930.7 pg/mL], $P < 0.05$; Table 1). Vitreous MCP-1 concentrations were significantly higher in patients receiving ARB treatment than in those not receiving ARB treatment (1,604.9 pg/mL [284.3–7,823.3 pg/mL] vs. 898.4 pg/mL [35.6–5,780.5 pg/mL], $P < 0.05$; Table 1).

Similarly, vitreous IL-8 concentrations (median [range]) were significantly higher in hypertensive patients than in nonhypertensive patients (38.9 pg/mL [3.2–314.3 pg/mL] vs. 20.3 pg/mL [1.0–139.7 pg/mL], $P < 0.05$; Table 2). Vitreous IL-8 concentrations (median [range]) were also significantly higher in patients with active diabetic retinopathy than in those with inactive diabetic retinopathy (44.3 pg/mL [1.0–314.3 pg/mL] vs. 12.9 pg/mL [4.2–37.5 pg/mL], $P < 0.01$; Table 2). Vitreous IL-8 concentrations (median [range]) were significantly higher in patients receiving ARB treatment than in those not receiving ARB

Table 1. Comparison of Vitreous MCP-1 Concentrations Between 2 Subgroups of Subjects with Diabetic Retinopathy Divided by Sex or Various Clinical Parameters

Clinical Parameter	Vitreous MCP-1 (pg/mL), Median (Range)	*P* (Wilcoxon Rank Sum Test)
Sex		
Men (n = 25)	1,266.9 (35.6–7,823.3)	0.091
Women (n = 16)	934.6 (284.3–2,359.3)	
Diabetes type		
Type 1 (n = 4)	951.4 (36.6–7,823.3)	0.223
Type 2 (n = 37)	2,088.1 (1,200.4–5,780.5)	
Insulin use		
No (n = 18)	1,267.1 (364.3–5,941.4)	0.623
Yes (n = 23)	1,095.0 (35.6–7,823.3)	
Hypertension		
No (n = 17)	865.5 (35.5–5,780.5)	0.028
Yes (n = 24)	1,597.7 (284.3–7,823.3)	
Hyperlipidemia		
No (n = 25)	1,266.9 (35.6–7,823.3)	0.893
Yes (n = 16)	948.0 (379.7–4,434.2)	
Proteinuria		
No (n = 12)	825.3 (35.6–5,941.4)	0.053
Yes (n = 29)	1,483.8 (379.7–7,823.3)	
Diabetic retinopathy		
Inactive (n = 11)	614.3 (35.6–2,930.7)	0.042
Active (n = 30)	1,428.7 (456.4–7,823.3)	
ARB treatment		
No (n = 20)	898.4 (35.6–5,780.5)	0.023
Yes (n = 21)	1,604.9 (284.3–7 823.3)	
Calcium channel blocker treatment		
No (n = 26)	970.5 (35.6–7,823.3)	0.233
Yes (n = 15)	1,590.5 (364.0–5,941.4)	

Table 2. Comparison of Vitreous IL-8 Concentrations Between 2 Subgroups of Subjects with Diabetic Retinopathy Divided by Sex or Various Clinical Parameters

Clinical Parameter	Vitreous IL-8 (pg/mL), Median (Range)	*P* (Wilcoxon Rank Sum Test)
Sex		
Men (n = 25)	36.7 (4.2–314.3)	0.173
Women (n = 16)	19.9 (1.0–187.5)	
Diabetes type		
Type 1 (n = 4)	24.0 (1.0–314.3)	0.291
Type 2 (n = 37)	42.8 (31.8–139.7)	
Insulin use		
No (n = 18)	24.2 (4.2–314.3)	0.609
Yes (n = 23)	34.3 (1.0–84.1)	
Hypertension		
No (n = 17)	20.3 (1.0–139.7)	0.047
Yes (n = 24)	38.9 (3.2–314.3)	
Hyperlipidemia		
No (n = 25)	31.8 (3.2–314.2)	0.894
Yes (n = 16)	30.2 (1.0–229.7)	
Proteinuria		
No (n = 12)	18.1 (3.2–100.9)	0.165
Yes (n = 29)	36.7 (1.0–314.3)	
Diabetic retinopathy		
Inactive (n = 11)	12.9 (4.2–37.5)	0.005
Active (n = 30)	44.3 (1.0–314.3)	
ARB treatment		
No (n = 20)	21.8 (1.0–225.5)	0.033
Yes (n = 21)	40.4 (4.4–314.3)	
Calcium channel blocker treatment		
No (n = 26)	23.9 (1.0–314.3)	0.223
Yes (n = 15)	40.3 (3.2–251.0)	

treatment (40.3 pg/mL [4.4–314.3 pg/mL] vs. 21.8 pg/mL [1.0–225.5 pg/mL], $P < 0.05$; Table 2).

Vitreous levels (median [range]) of VEGF (474.7 pg/mL [10.4–2,877.0 pg/mL] vs. 221.6 pg/mL [21.0–655.3 pg/mL], $P = 0.095$), IP-10 (286.3 pg/mL [33.3–1,000.3 pg/mL] vs. 308.8 pg/mL [44.6–899.2 pg/mL], $P = 0.791$), and Mig (217.8 pg/mL [20.6–997.2 pg/mL] vs. 174.1 pg/mL [25.7–873.9 pg/mL], $P = 0.397$) were not significantly different between hypertensive and nonhypertensive patients.

Subsequently, the correlation between vitreous MCP-1 and IL-8 levels with clinical parameters was analyzed. In univariate analyses, both vitreous MCP-1 and IL-8 levels correlated negatively with age (n = 41; MCP-1, $R^2 = -0.41$; IL-8, $R^2 = -0.38$, $P < 0.05$ for both; Table 3). Vitreous MCP-1 level correlated positively with systolic blood pressure ($R^2 = 0.38$, $P < 0.05$; Table 3). Systolic blood pressure (median [range]) in hypertensive patients (140 mmHg [110–172 mmHg]) was significantly ($P = 0.008$) higher than that in nonhypertensive patients (120 mmHg [110–143 mmHg]).

In multivariate models using stepwise multiple regression analysis, age ($P = 0.028$ and $P = 0.034$, respectively), active diabetic retinopathy ($P = 0.004$ and $P = 0.007$, respectively), systolic blood pressure ($P = 0.039$ and $P = 0.041$, respectively), hypertension ($P = 0.032$ and $P = 0.035$, respectively), and ARB treatment ($P = 0.039$ and $P = 0.028$, respectively) were significant and independent predictors for increased vitreous MCP-1 and IL-8 levels.

Discussion

In the present study of patients with diabetic retinopathy, we demonstrated the following findings: 1) vitreous levels of MCP-1 and IL-8 were significantly elevated in patients with concurrent hypertension compared with patients without hypertension; 2) vitreous levels of MCP-1 and IL-8 were significantly elevated in patients with active diabetic retinopathy compared with those with inactive diabetic retinopathy; 3) vitreous MCP-1 levels correlated with both age and systolic blood pressure; and 4) age, active diabetic retinopathy, systolic blood pressure, and hypertension were significant and independent predictors for increased vitreous MCP-1 and IL-8 concentrations. These findings indicate that systemic

Table 3. Correlations of Vitreous MCP-1 and IL-8 Concentrations with Age and Various Clinical Parameters

Clinical Parameter (n = 41)	Median (Range)	Correlation with Vitreous MCP-1		Correlation with Vitreous IL-8	
		R^2	*P*	R^2	*P*
Age (years)	63 (27–78)	−0.41	0.011	−0.38	0.017
Hemoglobin A_{1C} (%)	6.7 (5.0–12.0)	−0.25	0.114	0.785	0.04
Systolic blood pressure (mmHg)	135 (110–172)	0.38	0.019	0.29	0.074
Diastolic blood pressure (mmHg)	70 (54–100)	0.31	0.077	0.31	0.069
Total cholesterol (mg/dL)	200 (85–293)	−0.23	0.163	−0.21	0.205
Creatinine (mg/dL)	0.9 (0.5–8.7)	0.26	0.126	0.05	0.755

Spearman rank correlation test was used in the analyses.

hypertension is associated with elevated vitreous levels of both MCP-1 and IL-8 in diabetic retinopathy. The increased vitreous levels of the cytokines are unlikely to be because of breakdown of the blood–retinal barrier or contamination from blood as a result of vitreous hemorrhage in diabetic retinopathy, because we demonstrated in our previous study that the vitreous levels were significantly and markedly higher than serum levels and there was no correlation between serum and vitreous levels of these cytokines.[15]

The Wisconsin Epidemiologic Study of Diabetic Retinopathy, a long-term cohort and population-based incidence study, concluded that the presence of not only hyperglycemia but also hypertension is associated with an increase in the risk of progression to proliferative diabetic retinopathy and to the incidence of macular edema.[11] The UK Prospective Diabetes Study, a multicenter and randomized controlled trial, concluded that a strict blood pressure control policy, in comparison with a less strict blood pressure control policy, reduces the risk of clinical complications from diabetic eye disease.[12] These epidemiologic studies clearly identify systemic hypertension as an independent risk factor for diabetic retinopathy. There are no definite data to explain why high blood pressure is detrimental to the progression of diabetic retinopathy. Retinal blood flow is controlled by normal vasoconstriction through autoregulation. Retinal blood flow is increased, however, in patients with diabetic retinopathy, and the autoregulatory system is impaired in long-standing diabetes mellitus.[19] Because systemic hypertension increases vascular shear stress, the UK Prospective Diabetes Study group speculated that increased shear stress because of increased blood pressure may damage retinal vessel walls and worsen diabetic retinopathy.[12] When experimental hypertension was induced in diabetic subjects, retinal blood flow was significantly increased by an impairment of vascular autoregulation in response to both elevated systemic blood pressure and blood glucose levels.[20] Because vascular tissues are constantly subjected to shear stress from blood flow and strain induced by blood pressure, increased retinal vascular damage caused by shear stress or increased mechanical stretch caused by high blood pressure may be the major reason for the progression of diabetic retinopathy in patients with concurrent hypertension.

Monocyte chemotactic protein 1 and IL-8 are members of the chemokine family and are small molecular cytokines that induce both chemotaxis and chemokinesis in specific leukocyte populations. Monocyte chemotactic protein 1 belongs to the C-C subfamily and is a potent chemoattractant for monocyte recruitment.[5] Interleukin 8 belongs to the C-X-C subfamily and is mainly active on neutrophils.[6] Markedly increased MCP-1 and IL-8 are detected in the vitreous of patients with diabetic retinopathy.[7,8,15,21–23] Inflammatory chemokines are potentially angiogenic factors.[9,10,24,25] Therefore, MCP-1 and IL-8 levels may promote intraocular angiogenesis and act together to cause neovascularization in diabetic retinopathy. However, hypertension is associated with vascular inflammatory responses and is a major risk factor for the development of atherosclerosis.[26] Chronic leukocyte-mediated inflammation in the vascular walls is also observed in hypertensive patients and experimental animals.[27,28] The constant shear stress on endothelial cells resulting from mechanical forces on the vascular wall, such as blood flow and strain induced by blood pressure, may modulate the secretion of various proteins. Upregulation of MCP-1 and IL-8 expression is detected in the aortic tissues of hypertensive rats, and treatment with antihypertensive medication markedly reduces MCP-1 and IL-8 expression.[13,14] In addition, in vitro studies demonstrated that cyclic stretching enhances the secretion and gene expression of MCP-1 and IL-8 in a stretch-dependent manner in cultured endothelial cells of human umbilical veins.[29,30] These results suggest that MCP-1 and IL-8 are involved in hypertensive inflammatory changes in human vascular walls. Suzuma et al[31] demonstrated that exposure of bovine retinal endothelial cells to cyclic stretching upregulated the expression of VEGF and its receptor, whereas retinal expressions of VEGF and its receptors were also increased in spontaneously hypertensive rats. To our knowledge, however, there have been no reports on the expression of MCP-1 and IL-8 in retinal endothelial cells subjected to cyclic stretching or in retinal vessels of hypertensive animal. The present study is the first to document a significant increase in intraocular MCP-1 and IL-8 in hypertensive patients compared with nonhypertensive patients. Vitreous MCP-1 levels also correlated with systolic blood pressure, and systolic blood pressure and hypertension were identified as independent predictors for increases in both vitreous MCP-1 and IL-8 concentrations. These findings together suggest that systemic hypertension may induce MCP-1 and IL-8 overexpression in retinal vascular tissue, thereby increasing levels of both MCP-1 and IL-8 in the vitreous of hypertensive patients with diabetic retinopathy. Further in vitro and in vivo studies are required to verify this notion.

Our analyses also demonstrated that active diabetic retinopathy and age are significant and independent factors that influence vitreous MCP-1 and IL-8 levels. Elner et al[8] and Mitamura et al[22] measured vitreous

concentrations of MCP-1 and IL-8 in patients with diabetic retinopathy and reported higher concentrations of both chemokines in the vitreous of patients with active diabetic retinopathy compared with patients with inactive diabetic retinopathy. Although these previous results support our finding regarding active diabetic retinopathy, an association of age with vitreous MCP-1 and IL-8 concentrations has not been reported previously. In the present analysis, these two chemokines were elevated to a greater extent in the diabetic vitreous of younger patients than that of older patients. The reason for this finding is unknown, but this may verify the clinical observation that young diabetic adults tend to have more severe diabetic retinopathy.[32]

The renin–angiotensin system plays an important role in the regulation of systemic blood pressure. Recent experimental and clinical studies reported an association between the renin–angiotensin system and diabetic retinopathy. Funatsu et al[33] measured vitreous concentrations of Angiotensin II in patients with diabetic macular edema and reported higher concentrations of Angiotensin II in the vitreous of patients with hyperfluorescent diabetic macular edema compared with those with hypofluorescence. The induction of diabetes in mice led to an increase in retinal expression and production of the renin–angiotensin system components including Angiotensin II and its receptor, and the administration of ARBs inhibited diabetes-induced retinal expression of VEGF.[34] In murine brain–derived capillary endothelial cells stimulated with a high concentration of glucose, upregulation of MCP-1 is suppressed by ARB.[34] Clinically, treatment with an angiotensin-converting enzyme inhibitor reduces both the incidence and progression of diabetic retinopathy in Type 1 diabetic patients without concurrent hypertension.[35] Treatment with ARB also improves diabetic retinopathy in Type 2 diabetic patients without hypertension.[36] Approximately 90% of our hypertensive subjects were being treated with an ARB. Therefore, these previous reports do not necessarily support our findings of higher vitreous concentrations of MCP-1 and IL-8 in the ocular tissue of patients receiving ARB treatment. It is possible that systemic ARB treatment does not affect the vitreous MCP-1 and IL-8 levels sufficiently to lower the vitreous concentrations in patients with diabetic retinopathy or that ARB is not involved in the suppression of chemokines in diabetic ocular tissues.

A limitation of the present study was the few patients. Further clinical and experimental studies are required to elucidate the association of diabetic retinopathy with hypertension and of diabetic retinopathy with ARB. In conclusion, the findings of the present study may help to explain the epidemiologic and clinical evidence that systemic hypertension exacerbates diabetic retinopathy.

Key words: chemokine, diabetic retinopathy, hypertension, interleukin 8, monocyte chemotactic protein 1, vitreous.

References

1. Frank RN. Diabetic retinopathy. N Engl J Med 2004;50:48–58.
2. Stanford MR. The pathogenesis of diabetic retinopathy. Br J Ophthalmol 2004;88:444–445.
3. Barouch FC, Miyamoto K, Allport JR, et al. Integrin-mediated neutrophil adhesion and retinal leukostasis in diabetes. Invest Ophthalmol Vis Sci 2000;41:1153–1158.
4. Joussen AM, Murata T, Tsujikawa A, et al. Leukocyte-mediated endothelial cell injury and death in the diabetic retina. Am J Pathol 2001;158:147–152.
5. Matsushima K, Larsen CG, DuBois GC, Oppenheim JJ. Purification and characterization of a novel monocyte chemotactic and activating factor produced by a human myelomonocytic cell line. J Exp Med 1989;169:1485–1490.
6. Larsen CG, Anderson AO, Appella E, et al. The neutrophil-activating protein (NPA-1) is also chemotactic for T lymphocytes. Science 1989;243:1464–1466.
7. Capeans C, Rojas MV, Lojo S, Salorio MS. C-C chemokines in the vitreous of patients with proliferative vitreoretinopathy and proliferative diabetic retinopathy. Retina 1998;18:546–550.
8. Elner SG, Strieter RM, Bian ZM, et al. Interferon-induced protein 10 and interleukin 8 C-X-C chemokines present in proliferative diabetic retinopathy. Arch Ophthalmol 1998;116:1597–1601.
9. Koch AE, Polverini PJ, Kunkel SL, et al. Interleukin-8 as a macrophage-derived mediator of angiogenesis. Science 1992;258:1798–1801.
10. Strieter RM, Polverini PJ, Kunkel SL, et al. The functional role of the ELR motif in CXC chemokine-mediated angiogenesis. J Biol Chem 1995;270:27348–27357.
11. Klein R, Klein BE, Moss SE, Cruickshanks KJ. The Wisconsin epidemiologic study of diabetic retinopathy: XVII. The 14-year incidence and progression of diabetic retinopathy and associated risk factors in type 1 diabetes. Ophthalmology 1998;105:1801–1815.
12. UK Prospective Diabetes Study (UKPDS) group. Risk of progression of retinopathy and vision loss related to tight blood pressure control in type 2 diabetes mellitus. UKPDS 69. Arch Ophthalmol 2004;122:1631–1640.
13. Capers Q 4th, Alexander RW, Lou P, et al. Monocyte chemoattractant protein-1 expression in aortic tissues of hypertensive rats. Hypertension 1997;30:1397–1402.
14. Kim HY, Kang YJ, Song IH, et al. Upregulation of interleukin-8/CXCL8 in vascular smooth muscle cells from spontaneously hypertensive rats. Hypertens Res 2008;31:515–523.
15. Wakabayashi Y, Usui Y, Okunuki Y, et al. Correlation of vascular endothelial growth factor with chemokines in the vitreous in diabetic retinopathy. Retina 2010;30:339–344.
16. The Hypertension Detection and Follow-up Program. Hypertension detection and follow-up program cooperative group. Prev Med 1976;5:207–215.
17. Japanese Society of Hypertension. Japanese Society of Hypertension guidelines for the management of hypertension (JSH 2004). Hypertension Res 2006;29:S1–S106.

18. Wakabayashi Y, Usui Y, Okunuki Y, et al. Increased levels of monokine induced by interferon-γ (Mig) in the vitreous of patients with diabetic retinopathy. Diabet Med 2008;25: 875–877.
19. Grunwald JE, Riva CE, Sinclair SF, et al. Laser Doppler velocimetry study of retinal circulation in diabetes mellitus. Arch Ophthalmol 1986;104:991–996.
20. Rassam SM, Patel V, Kohner EM. The effect of experimental hypertension on retinal vascular autoregulation in humans: a mechanism for the progression of diabetic retinopathy. Exp Physiol 1995;80:53–68.
21. Elner SG, Elner VM, Jaffe GJ, et al. Cytokines in proliferative diabetic retinopathy and proliferative vitreoretinopathy. Curr Eye Res 1995;14:1045–1053.
22. Mitamura Y, Takeuchi S, Matsuda A, et al. Monocyte chemotactic protein-1 in the vitreous of patients with proliferative diabetic retinopathy. Ophthalmologica 2001; 215:415–418.
23. Funatsu H, Noma H, Mimura T, et al. Association of vitreous inflammatory factors with diabetic macular edema. Ophthalmology 2009;116:73–79.
24. Belperio JA, Keane MP, Arenberg DA, et al. CXC chemokines in angiogenesis. J Leukoc Biol 2000;68:1–8.
25. Yoshida S, Yoshida A, Ishibashi T, et al. Role of MCP-1 and MIP-1α in retinal neovascularization during postischemic inflammation in a mouse model of retinal neovascularization. J Leukoc Biol 2003;73:137–144.
26. Alexander RW. Hypertension and the pathogenesis of atherosclerosis. Hypertension 1995;25:155–161.
27. Ishibashi M, Hiasa KI, Zhao Q, et al. Critical role of monocyte chemoattractant protein-1 receptor CCR2 on monocyte in hypertension-induced vascular inflammation and remodeling. Circ Res 2004;94:1203–1210.
28. Parissis JT, Korovesis S, Giazizoglou E, et al. Plasma profile of peripheral monocyte-related inflammatory markers in patients with arterial hypertension. Correlation with plasma endothelin-1. Inv J Cardiol 2002;83:13–21.
29. Wung BS, Cheng JJ, Chao YJ, Wang DL. Cyclic strain increases monocyte chemotactic protein-1 secretion in human endothelial cells. Am J Physiol 1996;270:1462–1468.
30. Okada M, Matsumori A, Ono K, et al. Cyclic stretch upregulates production of interleukin-8 and monocyte chemotactic and activating factor/monocyte chemoattractant protein-1 in human endothelial cells. Arterioscler Thromb Vasc Biol 1998;18:894–901.
31. Suzuma I, Hata Y, Clermont A, et al. Cyclic stretch and hypertension induced retinal expression of vascular endothelial growth factor and vascular endothelial growth factor receptor-2. Potential mechanisms for exacerbation of diabetic retinopathy by hypertension. Diabetes 2001;50:444–454.
32. Lewis M, Abrams GW, Williams GA. Anterior hyaloidal fibrovascular proliferation after vitrectomy. Am J Ophthalmol 1987;104:607–613.
33. Funatsu H, Yamashita H, Ikeda T, et al. Angiotensin II and vascular endothelial growth factor in the vitreous fluid of patients with diabetic macular edema and other retinal disorders. Am J Ophthalmol 2002;133:537–543.
34. Nagai N, Izumi-Nagai K, Oike Y, et al. Suppression of diabetes-induced retinal inflammation by blocking the angiotensin II type 1 receptor or its downstream nuclear factor-κB pathway. Invest Ophthalmol Vis Sci 2007;48:4342–4350.
35. Chaturvedi N, Sjolie AK, Stephenson JM, et al. Effect of lisinopril on progression of retinopathy in normotensive people with type 1 diabetes. The EUCLID study group. EURODIAB control trial of lisinopril in insulin-dependent diabetes mellitus. Lancet 1998;351:28–31.
36. The DIRECT Programme Study Group. Effect of candesartan on progression and regression of retinopathy in type 2 diabetes (DIRECT-Protect 2): a randomized placebo-controlled trial. Lancet 2008;372:1385–1393.

Graefes Arch Clin Exp Ophthalmol (2011) 249:1485–1492
DOI 10.1007/s00417-011-1708-7

BASIC SCIENCE

Choroidal thickness measurement in healthy Japanese subjects by three-dimensional high-penetration optical coherence tomography

Tetsuya Agawa · Masahiro Miura · Yasuhi Ikuno · Shuichi Makita · Tapio Fabritius · Takuya Iwasaki · Hiroshi Goto · Kohji Nishida · Yoshiaki Yasuno

Received: 15 January 2011 / Revised: 12 April 2011 / Accepted: 18 April 2011 / Published online: 10 May 2011

Abstract
Background We performed retinal and choroidal thickness mapping by three-dimensional high-penetration optical coherence tomography (OCT) and evaluated the choroidal thickness distribution throughout the macula in healthy eyes.

Methods Forty-three eyes of 43 healthy Japanese volunteers were evaluated by 1060-nm swept-source OCT. The eyes were scanned with a three-dimensional raster scanning protocol, and the mean retinal and choroidal thicknesses of the posterior sectors were obtained. The sectors were defined by the Early Treatment Diabetic Study (ETDRS) layout. These data were compared by age (23–56 years), spherical equivalent refractive error (between +0.9 D and −10.3 D), and axial length (22.9–27.6 mm).

Results The mean retinal and choroidal thicknesses of the ETDRS area were 284±14 μm and 348±63 μm respectively. The mean regional choroidal thicknesses in the nasal inner macula and nasal outer macula were significantly smaller than those in all other sectors. The mean regional choroidal thickness in most sectors showed a significant negative correlation with axial length and a significant positive correlation with refractive error. In eyes with a long axial length (>25.0 mm), the mean regional choroidal thickness of five sectors showed a significant negative correlation with age. The coefficient of variation of choroidal thickness between sectors showed a significant negative correlation with axial length, and a positive correlation with refractive error. The mean retinal thickness in each sector was not significantly correlated with the mean choroidal thickness, age, axial length, or refractive error.

Conclusions The choroidal thickness map showed a distribution entirely different from the retinal thickness map. Choroidal thickness varies significantly with location, axial length, refractive error, and age. These variations should be considered when evaluating choroidal thickness.

Keywords Choroidal thickness · Optical coherence tomography · Three-dimensional mapping · Early Treatment Diabetic Retinopathy Study

Tetsuya Agawa and Masahiro Miura contributed equally to this study.

T. Agawa · M. Miura (✉) · T. Iwasaki
Department of Ophthalmology, Tokyo Medical University,
Ibaraki Medical Center,
3-20-1 Chuo, Ami,
Inashiki, Ibaraki 3000395, Japan
e-mail: m-miura@tokyo-med.ac.jp

M. Miura · S. Makita · Y. Yasuno
Computational Optics and Ophthalmology Group,
1-1-1 Tennodai,
Tsukuba, Ibaraki 3058577, Japan

Y. Ikuno · K. Nishida
Department of Ophthalmology, Osaka University Medical School,
2–2 Yamadaoka, Suita,
Osaka 5650871, Japan

S. Makita · Y. Yasuno
Computational Optics Group, University of Tsukuba,
1-1-1 Tennodai,
Tsukuba, Ibaraki 3058577, Japan

T. Fabritius
Optoelectronics and Measurement Techniques Laboratory,
University of Oulu,
PO Box 4500, 90014 Oulu, Finland

H. Goto
Department of Ophthalmology, Tokyo Medical University,
6-7-1 Nishishinjuku, Shinjuku-ku,
Tokyo 1600023, Japan

Introduction

The choroid is an important tissue that supplies blood to the outer retina; a deficiency in choroidal vascular supply leads to retinal dysfunction and visual loss [1]. Choroidal abnormalities are thought to be crucial for the pathogenesis of various chorioretinal diseases such as age-related macular degeneration and Vogt–Koyanagi–Harada disease [2, 3]. Precise measurements of choroidal thickness are essential to evaluate the pathophysiological changes in these diseases. Recent advances in optical interferometry have enabled micrometer-scale measurements of choroidal thickness. Partial coherence interferometry may be used to measure choroidal thickness at the fovea [4]. Enhanced depth imaging with commercial optical coherence tomography (OCT) at 840 nm provides two-dimensional line tomography and thickness of the choroid [5, 6]. OCT using a 1-μm probe wavelength, the so-called high-penetration OCT, enables choroidal thickness measurement at arbitrary points in the macula [7–9]. These studies used point-by-point measurements to provide important information regarding choroidal thickness [4–6, 8, 9]. High-penetration OCT can provide three-dimensional choroidal tomography.

For the evaluation of macular disease, a comprehensive evaluation of choroidal thickness across the entire macula may be important. Use of the Early Treatment Diabetic Retinopathy Study (ETDRS) layout is a standard protocol for comprehensive evaluation of the entire macula when measuring retinal thickness by commercial OCT [10–13]. With regard to the compatibility of retinal thickness measurement with choroidal thickness measurement, choroidal thickness mapping with the ETDRS layout could be a sensible method for comprehensive evaluation of the entire macula. In this study, we performed choroidal thickness mapping in the ETDRS layout by high-penetration OCT, and evaluated the three-dimensional choroidal thickness distribution in healthy eyes.

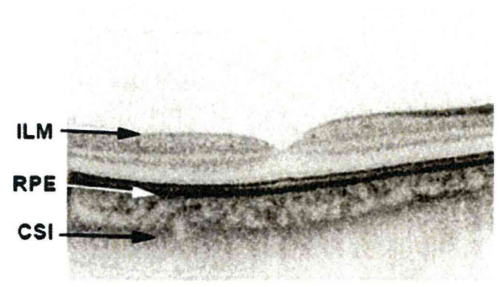

Fig. 1 A typical B-scan optical coherence tomography (OCT) image of a 1060-nm swept-source OCT. The retina and choroid are defined as the space between the internal limiting membrane (*ILM*) and the retinal pigment epithelium (*RPE*) and the space between the RPE and the chorioscleral interface (*CSI*) respectively

Materials and methods

Subjects

Forty-three eyes of 43 healthy Japanese volunteers, including 37 males and six females, aged 23–56 years (mean age: 32.9±8.5 years) were included in the analysis. Exclusion criteria included a history of any intraocular surgery, retinal pathology, choroidal pathology, glaucoma, tilted disc syndrome, or systemic disease such as diabetes mellitus or hypertension. Spherical equivalent refractive error was measured using an autorefractometer (ARK-530A; Nidek, Gamagori, Japan), and axial length was measured by partial coherence interferometry (IOLMaster; Carl Zeiss Meditec, La Jolla, CA, USA). The mean refractive error was −3.5± 3.0 D (range: +0.8 to −10.4 D), and the mean axial length was 25.0±1.4 mm (range: 22.9–27.6 mm).

All experiments were performed according to the tenets of the Declaration of Helsinki and were approved by the Institutional Review Boards of Osaka University Medical School and Tokyo Medical University. Informed consent was obtained from all the subjects after explaining the nature and the possible consequences of the study.

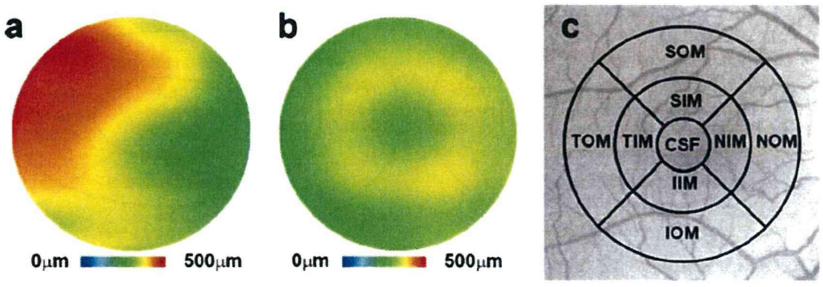

Fig. 2 Choroidal thickness map (**a**) and retinal thickness map (**b**) of the area corresponding to the Early Treatment Diabetic Retinopathy Study (ETDRS) layout area and nine sectors of the ETDRS layout (**c**). *CSF*: central subfield, *NIM*: nasal inner macula, *SIM*: superior inner macula, *TIM*: temporal inner macula, *IIM*: inferior inner macula, *NOM*: nasal outer macula, *SOM*: superior outer macula, *TOM*: temporal outer macula, IOM: inferior outer macula

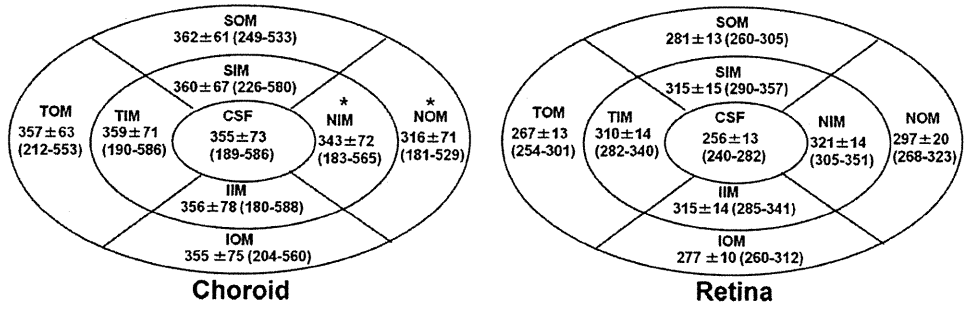

Fig. 3 The mean regional choroidal thickness {mean ± SD, (minimum–maximum)} and the mean regional retinal thickness map {mean ± SD, (minimum–maximum)} in the ETDRS layout for all 43 eyes. * $P<0.05$, *CSF*: central subfield, *NIM*: nasal inner macula, *SIM*: superior inner macula, *TIM*: temporal inner macula, *IIM*: inferior inner macula, *NOM*: nasal outer macula, *SOM*: superior outer macula, *TOM*: temporal outer macula, IOM: inferior outer macula

OCT measurement

The prototype swept-source OCT system was built by the Computational Optic Group at the University of Tsukuba. A detailed description of this system has been published [7, 8, 14]. The center wavelength of the probe beam was 1,060 nm. The measurement speed was 50,000 A-scans/s, and the depth resolution was measured to be 14.4 μm in air, which is equivalent to 10.4 μm in the tissue. The interferometer was attached to a semi-custom fundus-scanning head based on a 3-D OCT-1000 (Topcon Corp., Tokyo, Japan). Volumetric scans were performed with a raster-scanning protocol, with 512 A-scans ×256 B-scans covering a 6.0×6.0-mm region on the retina. The center of each volumetric measurement was adjusted to the center of the fovea. The acquisition speed of each measurement was 2.6 s/volume.

Retinal and choroidal thickness mapping

Three-dimensional thickness mapping of the retina and choroid was performed on the basis of manual segmentation of every fourth B-scan image; 64 B-scan images were used for three-dimensional mapping [9]. Segmentation was performed by an experienced OCT reader (T.A.) by using image manipulation software (GIMP 2.6) and a reader blinded for age, axial length, and refractive error. The retina was defined as the layer between the internal limiting membrane and the retinal pigment epithelium, and the choroid was defined as the layer between the retinal pigment epithelium and the chorioscleral interface (Fig. 1). The three-dimensional thickness map was fitted to a two-dimensional surface defined by a ninth order polynomial, to provide smoother choroidal and retinal thickness maps (Fig. 2). From these three-dimensional thickness maps of the retina and the choroid, the mean regional thickness was calculated for the nine sectors of the ETDRS layout (Fig. 2). The inner and outer rings had diameters of 1–3 mm and 3–6 mm respectively, and they were segmented into superior, inferior, temporal, and nasal quadrants. The individual sectors were referred to as the central subfield, nasal inner macula, superior inner macula, temporal inner macula, inferior inner macula, nasal outer macula, superior outer macula, temporal outer macula, and inferior outer macula. The mean thickness of each sector was compared in the context of patient age,

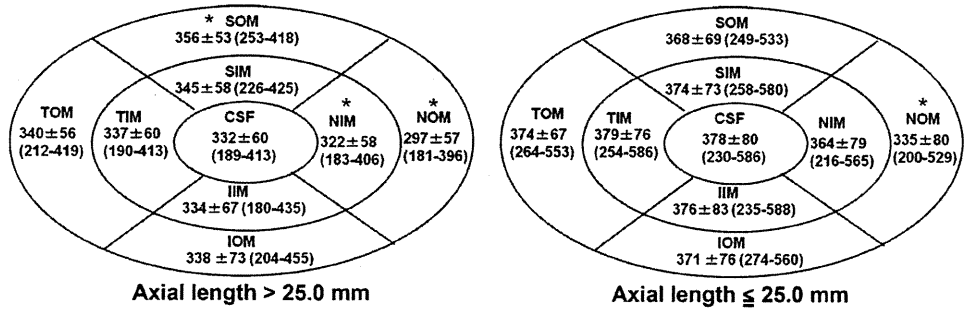

Fig. 4 The mean regional choroidal thickness {mean ± SD, (minimum–maximum)} in the ETDRS layout for eyes with an axial length longer than 25.0 mm (22 eyes) and ≤25.0 mm (21 eyes). * $P<0.05$, *CSF*: central subfield, *NIM*: nasal inner macula, *SIM*: superior inner macula, *TIM*: temporal inner macula, *IIM*: inferior inner macula, *NOM*: nasal outer macula, *SOM*: superior outer macula, *TOM*: temporal outer macula, IOM: inferior outer macula

Table 1 Correlation of the mean choroidal thickness at each sector with axial length, refractive error, and age

Axial length			Refractive error			Age		
Sector	R^2	P	Sector	R^2	P	Sector	R^2	P
CSF	−0.17	0.006	CSF	−0.14	0.01	CSF	0.01	0.48
NIM	−0.17	0.006	NIM	−0.14	0.01	NIM	0.01	0.45
SIM	−0.10	0.04	SIM	−0.10	0.04	SIM	0.001	0.85
TIM	−0.18	0.004	TIM	−0.18	0.006	TIM	0.01	0.52
IIM	−0.16	0.007	IIM	−0.16	0.007	IIM	0.01	0.49
NOM	−0.15	0.01	NOM	−0.14	0.01	NOM	0.01	0.43
SOM	−0.04	0.16	SOM	0.04	0.21	SOM	0.004	0.7
TOM	−0.18	0.005	TOM	0.16	0.007	TOM	0.003	0.76
IOM	−0.14	0.01	IOM	0.14	0.01	IOM	0.003	0.78
Total	−0.14	0.01	Total	0.14	0.01	Total	0.003	0.77

CSF, central subfield; NIM, nasal inner macula; SIM, superior inner macula; TIM, temporal inner macula; IIM, inferior inner macula; NOM, nasal outer macula; SOM, superior outer macula; TOM, temporal outer macula; IOM, inferior outer macula

refractive error, and axial length. To evaluate the potential effects of axial length, eyes were grouped into eyes with a long axial length (axial length >25.0 mm) and other eyes (axial length ≤25.0 mm), based on the normal axial length variation described in the literature [15].

Data were analyzed using a paired *t*-test and repeated-measures ANOVA to compare the thickness in different sectors, and by univariate regression analysis using a statistical software package (JMP, version 8.0.2.2; SAS Institute Inc, Cary, NC). *P* values less than 0.05 were considered significant.

Results

Good quality B-scan images were obtained for all the eyes; the delineation of the internal limiting membrane, retinal pigment epithelium, and chorioscleral interface was easily visualized for reliable thickness measurements. Accordingly, three-dimensional thickness maps of the retina and the choroid were created, and statistical analyses of the ETDRS layout could be readily performed.

The mean choroidal thickness of the whole ETDRS area was 348±63 μm (range: 217–544 μm), and the choroidal thickness of each sector showed large variation (Fig. 3). The mean regional choroidal thickness at the nasal inner macula and nasal outer macula was significantly smaller than that at all other sectors ($P<0.05$), and the mean regional choroidal thickness at the nasal outer macula was significantly smaller than that at the nasal inner macula ($P<0.0001$) (Fig. 3). In eyes with axial length longer than 25.0 mm (22 eyes), the mean regional choroidal thickness at the superior outer retina was greater than that at all the other sectors ($P<0.05$), and the mean regional choroidal thickness at the nasal inner macula and nasal outer macula was significantly smaller than that at all other sectors ($P<0.05$) (Fig. 4). In all other eyes (axial length ≤ 25.0 mm, 21 eyes), a significant difference was found only for the nasal outer macula, and the mean regional choroidal thickness at the nasal outer macula was significantly smaller than that at all other sectors ($P<0.05$) (Fig. 4).

The mean regional choroidal thickness at each sector showed a significant negative correlation with axial length ($P<0.05$, R^2: −0.18 to −0.10), except for the superior outer macula ($P=0.16$, $R^2=0.04$) (Table 1). The mean regional choroidal thickness at each sector showed a significant positive correlation with refractive error ($P<0.05$, R^2: 0.18–0.10), except for the superior outer macula ($P=0.21$, $R^2=0.036$) (Table 1). The mean choroidal thickness at each sector showed no significant correlation with age (Table 1). In eyes with a long axial length (> 25.0 mm, 22 eyes, mean age 30.2±5.4 years), the mean regional choroidal thickness at five sectors (central subfield, nasal inner macula, superior inner macula, temporal inner macula, and superior outer macula) showed a significant negative correlation with age ($P<0.05$, R^2: −0.20 to −0.33) (Table 2).

The mean retinal thickness of the entire ETDRS area was 284±14 μm (range: 268–318 μm). Among the ETDRS

Table 2 Correlation of the mean choroidal thickness at each sector with age for eyes with a long axial length (>25.0 mm)

Sector	R^2	P
CSF	−0.25	0.02
NIM	−0.21	0.04
SIM	−0.26	0.02
TIM	−0.20	0.04
IIM	−0.14	0.10
NOM	−0.14	0.10
SOM	−0.34	0.006
TOM	−0.14	0.10
IOM	−0.12	0.13
Total	−0.20	0.04

CSF, central subfield; NIM, nasal inner macula; SIM, superior inner macula; TIM, temporal inner macula; IIM, inferior inner macula; NOM, nasal outer macula; SOM, superior outer macula; TOM, temporal outer macula; IOM, inferior outer macula

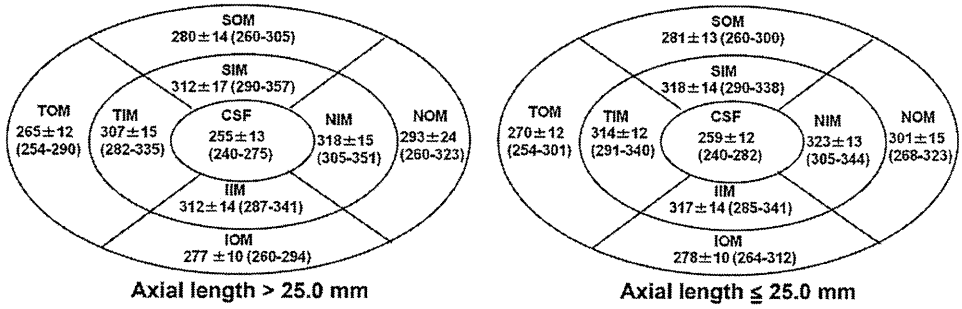

Fig. 5 The mean regional retinal thickness {mean ± SD, (minimum–maximum)} in the ETDRS layout for eyes with an axial length longer than 25.0 mm (22 eyes) and ≤25.0 mm (21 eyes). * $P<0.05$, *CSF*: central subfield, *NIM*: nasal inner macula, *SIM*: superior inner macula, *TIM*: temporal inner macula, *IIM*: inferior inner macula, *NOM*: nasal outer macula, *SOM*: superior outer macula, *TOM*: temporal outer macula, IOM: inferior outer macula

subfields, the nasal inner macula had the maximum retinal thickness (Fig. 3). The nasal inner macula also showed the maximum retinal thickness in eyes with a long axial length (>25.0 mm) and other eyes (axial length ≤ 25.0 mm) (Fig. 5). The mean retinal thickness at each sector did not show any significant correlation with age, axial length, refractive error, or the mean choroidal thickness at each sector (Table 3).

The coefficient of variation of the choroidal thickness between the sectors showed a significant positive correlation with axial length ($P=0.04$, $R^2=0.10$) and a negative correlation with refractive error ($P=0.01$, $R^2 = -0.16$) (Fig. 6). However, the coefficient of variation between sectors showed no significant correlation with age ($P=0.15$, $R^2=0.027$) (Fig. 6). The coefficient of variation of the retinal thickness between sectors did not show any significant correlation with age, axial length, or refractive error (Fig. 7).

Discussion

In this study, three-dimensional high-penetration OCT enabled comprehensive evaluation of retinal thickness and choroidal thickness in the whole macular area. The choroidal thickness map showed an entirely different distribution from that of the retinal thickness map. ETDRS mapping showed a diversity of the mean choroidal thickness by location, axial length, refractive error, and age. Choroidal thickness decreased nasally in all eyes, and was the greatest in the superior macular area in myopic eyes. Choroidal thickness was significantly correlated with axial length and refractive error. A significant correlation with age was observed in the myopic eyes.

This study showed a decrease in the choroidal thickness in the nasal direction, which is consistent with previous OCT studies [5, 8]. One possible reason for nasal choroidal thinning is the choroidal watershed zone that is frequently observed between the macula and optic disk [16]. Thinning at the nasal region, including the peripapillary area, may contribute to the vulnerability for pathological choroidal thinning in this area. Histologically, the choroid consists mostly of blood vessels; thus, a decrease in choroidal thickness represents a reduction in the choroid blood vessels [17]. From a clinical standpoint, choroidal thinning is thought to be representative of a decrease in the choroidal blood supply [18]. This vulnerability may be a cause of peripapillary atrophy in pathologic myopia and age-related

Table 3 Correlation of the mean retinal thickness with axial length, refractive error, age, and mean choroidal thickness in each sector

Axial length			Refractive error			Age			Choroidal thickness		
Sector	R^2	P	Sector	R^2	P	Sector	R^2	P	Sector	R^2	P
CSF	0.002	0.78	CSF	0.002	0.79	CSF	0.011	0.56	CSF	0.005	0.64
NIM	0.019	0.37	NIM	0.013	0.47	NIM	0.001	093	NIM	0.018	0.19
SIM	0.018	0.40	SIM	0.005	0.63	SIM	0.008	0.54	SIM	0.022	0.17
TIM	0.006	0.63	TIM	0.013	0.46	TIM	0.001	0.81	TIM	0.023	0.33
IIM	0.001	0.84	IIM	0.001	0.87	IIM	0.001	0.84	IIM	0.009	0.54
NOM	0.083	0.34	NOM	0.007	0.27	NOM	0.006	0.64	NOM	0.013	0.47
SOM	0.012	0.49	SOM	0.001	0.87	SOM	0.001	0.54	SOM	0.035	0.12
TOM	0.016	0.41	TOM	0.014	0.45	TOM	0.001	0.83	TOM	0.023	0.17
IOM	0.001	0.96	IOM	0.005	0.65	IOM	0.017	0.40	IOM	0.011	0.50
total	0.003	0..30	total	0.010	0.53	total	0.003	0.74	total	0.023	0.16

CSF, central subfield; NIM, nasal inner macula; SIM, superior inner macula; TIM, temporal inner macula; IIM, inferior inner macula; NOM, nasal outer macula; SOM, superior outer macula; TOM, temporal outer macula; IOM, inferior outer macula

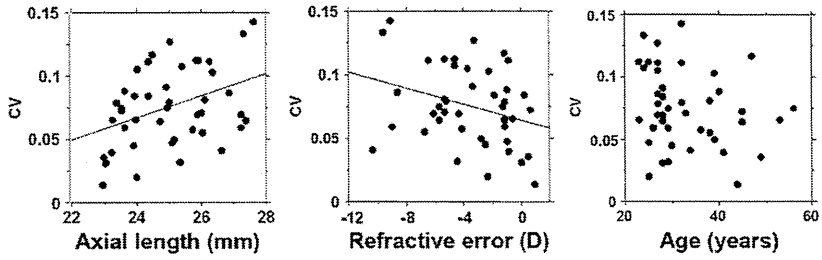

Fig. 6 Scatter plots of the coefficient of variation in choroidal thickness between ETDRS sectors for axial length, refractive error, and age

choroidal atrophy [18, 19]. In this study, choroidal thickness in myopic eyes decreased with age. This age-dependent decrease in the choroidal thickness may be related to the progressive disease status of pathologic myopia [19].

This study showed an increased coefficient of variation in the choroidal thickness between regional sectors in myopic eyes (Fig. 6). The distribution of choroidal thickness in the myopic eyes (axial length >25.0 mm) differed from that in other eyes (axial length ≤ 25.0 mm) (Fig. 4). These findings suggest that myopic choroidal changes occur asymmetrically in the macula. Disequilibrium in the choroidal thickness may be related to the focal alteration of the choroidal vasculature in highly myopic eyes [20]. To accurately evaluate the asymmetry of choroidal thickness, three-dimensional choroidal tomography with high-penetration OCT is better than two-dimensional line tomography by enhanced depth imaging.

This study did not show a significant correlation between choroidal thickness and age in all 43 subjects. Previous studies using OCT and a histopathologic study showed a negative correlation between age and choroidal thickness [5, 9, 21]. The narrow age distribution and the relatively young age in this study may be the cause of this discrepancy. Despite this limitation, a subgroup of myopic eyes showed a significant reduction in the choroidal thickness with age. This discrepancy may mean that the aging change of the choroidal thickness is more predominant in the myopic eyes than in the other eyes. A decrease in the choroidal blood flow is a crucial finding in pathologic myopia [20, 22–25]. This age-dependent decrease in choroidal thickness may be related to the progressive disease status of pathologic myopia [19]. Investigations with a large number of subjects of various ages are required to confirm the effects of the aging process on choroidal thickness.

Recently, enhanced-depth imaging OCT showed the clinical significance of choroidal thickness in various macular diseases [23, 26, 27]. These enhanced-depth imaging OCT studies were conducted by point-by-point measurement of choroidal thickness. Choroidal thickness varied across the entire macula. Point-by-point measurements may miss the overall character of choroidal thickness in the macula, and three-dimensional mapping is an appropriate method for comprehensive evaluation of the whole macular area. With high-speed high-penetration OCT, B-scans without image enhancement could be used for choroidal thickness measurement, and only a few seconds are required for three-dimensional measurement. In contrast, a few minutes are required for three-dimensional measurement with an enhanced-depth imaging OCT system. A high-speed high-penetration OCT is appropriate for three-dimensional choroidal thickness mapping.

In this study, choroidal thickness mapping showed large differences between the choroid and retinal thicknesses. Comparison of thickness maps between the choroid and retina may provide important information about chorioretinal disease. For appropriate comparison, the adoption of a uniform protocol is important. For objective evaluation of retinal thickness maps, the ETDRS layout is a standard protocol in commercial OCT [11–13]. Choroidal thickness mapping with the ETDRS layout is an appropriate method for maintaining fidelity with the retinal measurement, and is an optimum approach for comprehensive evaluation of the macular area.

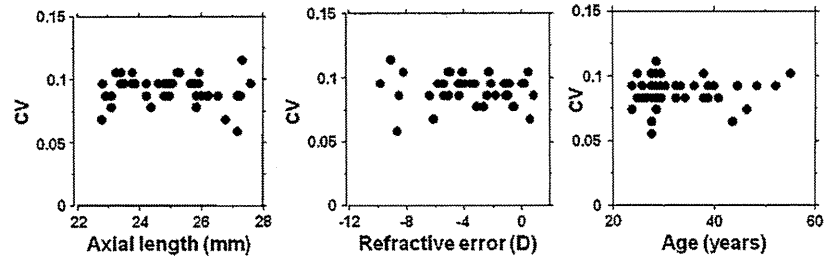

Fig. 7 Scatter plots of the coefficient of variation in retinal thickness between ETDRS sectors for axial length, refractive error, and age

Our study has some limitations. First, only 43 subjects were evaluated. Previous OCT studies of choroidal thickness have been conducted with less than 50 subjects, but choroidal thickness mapping showed a larger variation than retinal thickness mapping [5, 6, 8, 9, 11–13, 28, 29]. For the accurate evaluation of the large variation in choroidal thickness, a large number of subjects are required to establish a normal database. Second, at present, the choroid is manually segmented for three-dimensional choroidal thickness mapping [5, 6, 8, 9]. Manual segmentation may be suitable for point-by-point measurement; however, it requires a relatively long time for three-dimensional mapping. In this study, we used every fourth B-scan image to save segmentation time; however, segmentation time was still too long for clinical practice. With automatic segmentation, complete thickness mapping with whole volume data sets may be possible in clinical practice. Automatic measurements are required for more widespread use of choroidal thickness measurements.

At present, little is known about the significance of the thickness of the human choroid [1]. The choroid is involved in various vision-threatening ocular diseases. Comprehensive evaluation of the choroid with the ETDRS layout is helpful for understanding various ocular diseases, including age-related macular degeneration, pathologic myopia, and posterior uveitis [2, 3, 22, 23]. With the combination of other imaging modalities, such as indocyanine angiography, further investigations of various chorioretinal diseases may be possible. Choroidal thickness mapping with the ETDRS layout may function as a noninvasive assessment of chorioretinal diseases.

Acknowledgments This project was supported in part by the Japan Science and Technology Agency through the Development of Systems and Technology for Advanced Measurement and Analysis program.

Financial relationship Shuichi Makita: Topcon, Yoshiaki Yasuno: Topcon

References

1. Nickla DL, Wallman J (2010) The multifunctional choroid. Prog Retin Eye Res 29:144–168
2. McLeod DS, Grebe R, Bhutto I, Merges C, Baba T, Lutty GA (2009) Relationship between RPE and choriocapillaries in age-related macular degeneration. Invest Ophthalmol Vis Sci 50:4982–4991
3. Maruko I, Iida T, Sugano Y, Oyamada H, Sekiryu T, Fujiwara T, Spaide RF (2011) Subfoveal choroidal thickness after treatment of Vogt–Koyanagi–Harada disease. Retina 31:510–517
4. Brown JS, Flitcroft DI, Ying GS, Francis EL, Schmid GF, Quinn GE, Stone RA (2009) In vivo human choroidal thickness measurements: evidence for diurnal fluctuations. Invest Ophthalmol Vis Sci 50:5–12
5. Margolis R, Spaide RF (2009) A pilot study of enhanced depth imaging optical coherence tomography of the choroid in normal eyes. Am J Ophthalmol 147:811–815
6. Rahman W, Chen FK, Yeoh J, Patel P, Tufail A, Da Cruz L (2011) Repeatability of manual subfoveal choroidal thickness measurements in healthy subjects using the technique of enhanced depth imaging optical coherence tomography. Invest Ophthalmol Vis Sci 52:2267–2271
7. Yasuno Y, Miura M, Kawana K, Makita S, Sato M, Okamoto F, Yamanari M, Iwasaki T, Yatagai T, Oshika T (2009) Visualization of sub-retinal pigment epithelium morphologies of exudative macular diseases by high-penetration optical coherence tomography. Invest Ophthalmol Vis Sci 50:405–413
8. Ikuno Y, Kawaguchi K, Nouchi T, Yasuno Y (2010) Choroidal thickness in healthy Japanese subjects. Invest Ophthalmol Vis Sci 51:2173–2176
9. Esmaeelpour M, Povazay B, Hermann B, Hofer B, Kajic V, Kapoor K, Sheen NJ, North RV, Drexler W (2010) Three-dimensional 1060-nm OCT: choroidal thickness maps in normal subjects and improved posterior segment visualization in cataract patients. Invest Ophthalmol Vis Sci 51:5260–5266
10. Early Treatment Diabetic Retinopathy Study Research Group (1991) Early Treatment Diabetic Retinopathy Study design and baseline patient characteristics. ETDRS report number 7. Ophthalmology 98:741–756
11. Sull AC, Vuong LN, Price LL, Srinivasan VJ, Gorczynska I, Fujimoto JG, Schuman JS, Duker JS (2010) Comparison of spectral/Fourier domain optical coherence tomography instruments for assessment of normal macular thickness. Retina 30:235–245
12. Grover S, Murthy RK, Brar VS, Chalam KV (2009) Normative data for macular thickness by high-definition spectral-domain optical coherence tomography (spectralis). Am J Ophthalmol 148:266–271
13. Sayanagi K, Sharma S, Kaiser PK (2009) Comparison of retinal thickness measurements between three-dimensional and radial scans on spectral-domain optical coherence tomography. Am J Ophthalmol 148:431–438
14. Yasuno Y, Madjarova VD, Makita S, Akiba M, Morosawa A, Chong C, Sakai T, Chan K, Itoh M, Yatagai T (2005) Three-dimensional and high-speed swept-source optical coherence tomography for in vivo investigation of human anterior segments. Opt Express 13:10652–10664
15. Carney LG, Mainstone JC, Henderson BA (1997) Corneal topography and myopia. A cross-sectional study. Invest Ophthalmol Vis Sci 38:311–320
16. Hayreh SS (1990) In vivo choroidal circulation and its watershed zones. Eye (Lond) 4(Pt 2):273–289
17. Hogan MJ, Alvarado JA (1971) Histology of the human eye. Saunders, Philadelphia
18. Spaide RF (2009) Age-related choroidal atrophy. Am J Ophthalmol 147:801–810
19. Vongphanit J, Mitchell P, Wang JJ (2002) Prevalence and progression of myopic retinopathy in an older population. Ophthalmology 109:704–711
20. Moriyama M, Ohno-Matsui K, Futagami S, Yoshida T, Hayashi K, Shimada N, Kojima A, Tokoro T, Mochizuki M (2007) Morphology and long-term changes of choroidal vascular structure in highly myopic eyes with and without posterior staphyloma. Ophthalmology 114:1755–1762
21. Ramrattan R, van der Schaft T, Mooy C, de Bruijn W, Mulder P, de Jong P (1994) Morphometric analysis of Bruch's membrane, the choriocapillaries, and the choroid in aging. Invest Ophthalmol Vis Sci 35:2857–2864
22. Ikuno Y, Tano Y (2009) Retinal and choroidal biometry in highly myopic eyes with spectral-domain optical coherence tomography. Invest Ophthalmol Vis Sci 50:3876–3880
23. Fujiwara T, Imamura Y, Margolis R, Slakter JS, Spaide RF (2009) Enhanced depth imaging optical coherence tomography of the choroid in highly myopic eyes. Am J Ophthalmol 148:445–450

24. Grossniklaus HE, Green WR (1992) Pathologic findings in pathologic myopia. Retina 12:127–133
25. Ikuno Y, Jo Y, Hamasaki T, Tano Y (2010) Ocular risk factors for choroidal neovascularization in pathologic myopia. Invest Ophthalmol Vis Sci 51:3721–3725
26. Chung SE, Kang SW, Lee JH, Kim YT (2011) Choroidal thickness in polypoidal choroidal vasculopathy and exudative age-related macular degeneration. Ophthalmology. doi:10.1016/j.ophtha.2010.09.012
27. Maruko I, Iida T, Sugano Y, Ojima A, Ogasawara M, Spaide RF (2010) Subfoveal choroidal thickness after treatment of central serous chorioretinopathy. Ophthalmology 117:1792–1799
28. Manjunath V, Taha M, Fujimoto JG, Duker JS (2010) Choroidal thickness in normal eyes measured using Cirrus HD optical coherence tomography. Am J Ophthalmol 150:325–329
29. Benavente-Perez A, Hosking SL, Logan NS, Bansal D (2010) Reproducibility-repeatability of choroidal thickness calculation using optical coherence tomography. Optom Vis Sci 87:867–872

Correlation between high-resolution optical coherence tomography (OCT) images and histopathology in an *N*-methyl-*N*-nitrosourea—induced retinal degeneration rat model

Yasuyuki Yamauchi, Keisuke Kimura, Tsuyoshi Agawa, Rintaro Tsukahara, Maki Mishima, Naoyuki Yamakawa, Hiroshi Goto

Department of Ophthalmology, Tokyo Medical University Hospital, Tokyo, Japan

Correspondence to
Yasuyuki Yamauchi, Department of Ophthalmology, Tokyo Medical University Hospital, 6-7-1 Nishi-Shinjuku, Shinjuku-ku, Tokyo 160-0023, Japan; phthisis@nifty.com

Accepted 1 April 2011
Published Online First 20 April 2011

ABSTRACT

Background Recent research on macular diseases has prompted investigations into the condition of the intersection between the inner and outer segments (IS/OS), and its relationship with retinal photoreceptor abnormalities. Because the correlation between optical coherence tomography (OCT) images and histopathology is unclear, the authors compared them in an *N*-methyl-*N*-nitrosourea (MNU)-induced photoreceptor degeneration rat model.

Methods MNU (60 mg/kg), which is toxic to photoreceptors, was injected in 12 Brown Norway rats. After MNU administration, three rats were used per histopathological study 3 h, 6 h, 24 h and 1 week after the injections. Two healthy rats served as controls. OCT images were taken before euthanisation.

Results 3 h after the MNU injections, the IS and OS were oedematous, but the IS/OS borderline was recognised histopathologically, and the IS/OS was depicted on the OCT images. Six hours after injections, the OS were preserved, but the IS structures were destroyed or partially disorganised histopathologically, and the IS/OS was not observed on the OCT images. Twenty-four hours after the injections, the IS and OS were totally disorganised histopathologically, and the IS/OS was not depicted on the OCT images.

Conclusion The IS structure might be the origin of the IS/OS on OCT images.

INTRODUCTION

Optical coherence tomography (OCT) is a non-invasive, high-resolution alternative to ultrasound imaging that can be used to obtain cross-sectional images.[1] Drexler *et al* used OCT to observe the intersection of the inner and outer photoreceptor segments (IS/OS).[2] The IS/OS is recognised to play a key role in the visual prognosis of patients with macular diseases.[3–5] Although the accuracy with which OCT images can reflect histopathology in normal animals[6–10] and in several models of retinal diseases[11–13] has been verified, the use of OCT to show abnormal IS/OS has not been extensively investigated. In an earlier study, we hypothesised that when the IS/OS is not seen in OCT images, the IS structure has probably been destroyed, or the IS and OS may have disappeared entirely.[14] However, it has not been confirmed whether the IS/OS on OCT images accurately represents histopathology in animal models. In this study, we compared OCT images with retinal histopathology in an *N*-methyl-*N*-nitrosourea (MNU)-induced retinal degeneration rat model.[15 16]

MATERIALS AND METHODS

All experiments were performed in compliance with the ARVO Statement for the Use of Animals in Ophthalmic and Vision Research. Ethics permission was granted by the Tokyo Medical University Institutional Animal Care and Use Committee. Fourteen Brown Norway rats weighing approximately 0.2 kg were used. The animals received an intraperitoneal injection of sterile MNU (Sigma, St Louis, Missouri) at 60 mg/kg, a dose that can effectively cause photoreceptor degeneration.[15 16] A total of 24 eyes were available for OCT imaging, including three each from 3 h, 6 h, 24 h and 1 week after injection. Four healthy eyes of two rats served as controls. The rats were anaesthetised using intraperitoneal injections of pentobarbital (25 mg/kg). The pupils were dilated using 0.4% tropicamide and 0.5% phenylephrine. Subsequently, 0.1% hyaluronate sodium was applied to the eyes. OCT images were taken with a Cirrus HD-OCT (Carl Zeiss Meditec, Dublin, California). OCT images of a specific region of each eye were taken using the optic nerve head and photocoagulation as landmarks (figure 1A,C). OCT images with signal strength >8/10 in the Cirrus HD-OCT were selected for analysis. At the end of the study, the animals were euthanised with intravenous injections of pentobarbital (100 mg/kg). The eyes were enucleated, fixed by immersion in 4% paraformaldehyde in phosphate buffer and processed histopathologically using haematoxylin–eosin. Histopathological analysis was performed using the optic nerve head and photocoagulation scars as landmarks (figure 1B).

RESULTS

Histopathological analysis

We were able to observe clearly the IS and OS as well as the outer nuclear layers of the control retinas (figure 2A). Three hours after the injections, the structures of the IS and OS were relatively well preserved in retinas. The number of outer nuclei was preserved. The outer nuclei in MNU injected rats were stained as well as in control retinas. (figures 2B, 3A,B). Six hours after the injections, the IS were disorganised but the OS structures were

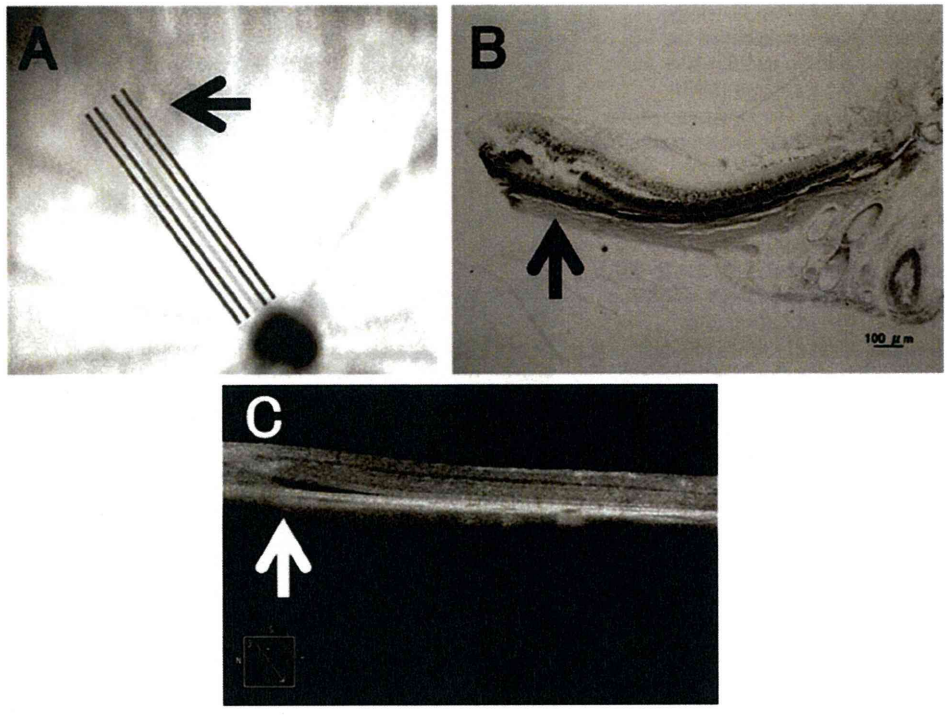

Figure 1 Landmarks marked by photocoagulation. (A) Fundus photograph obtained using Cirrus HD-OCT. Optical coherence tomography (OCT) scanning included the region of photocoagulation oedema and the optic disc. An arrow shows the region of photocoagulation oedema. (B) Histopathological observation. An arrow shows the region of photocoagulation oedema. (C) OCT image. An arrow shows the region of photocoagulation oedema.

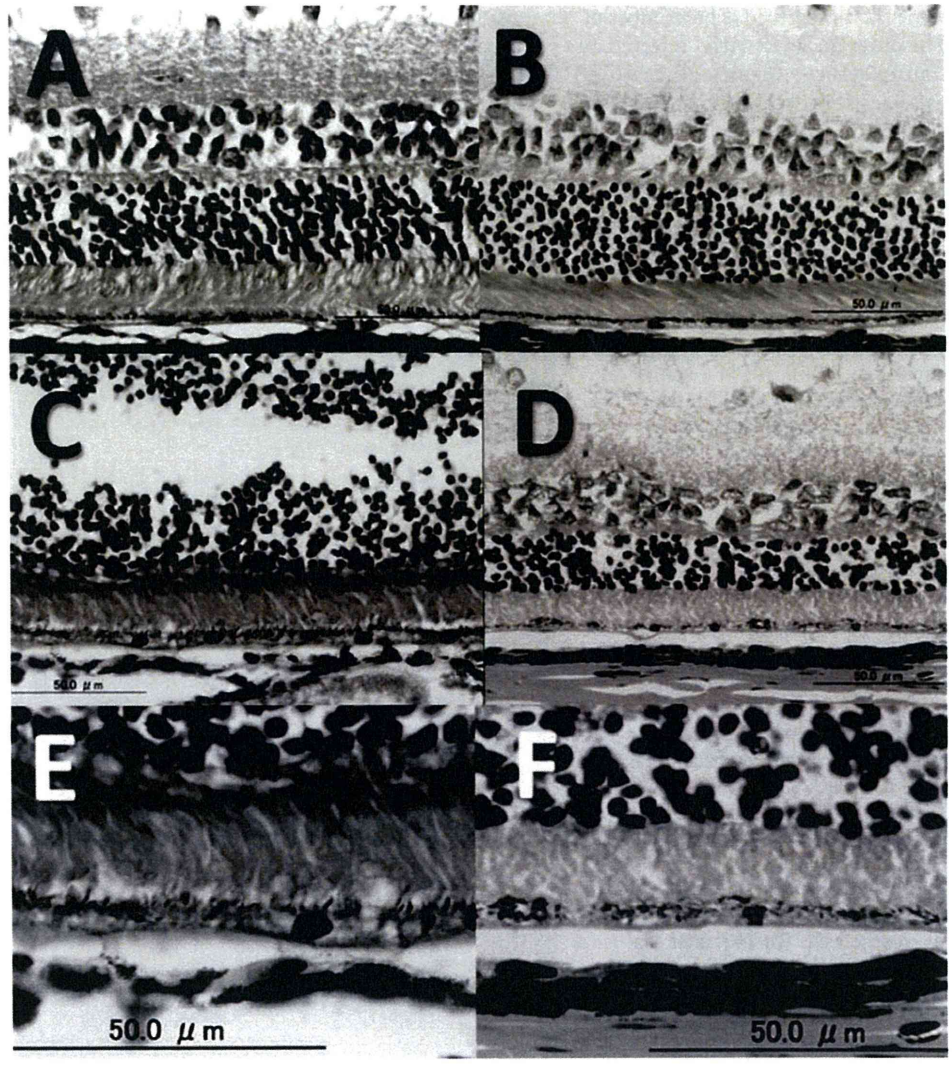

Figure 2 Histopathology of the retina in control and test rats injected with *N*-methyl-*N*-nitrosourea (MNU). (A) Normal rat. (B) 3 h after MNU injection, the photoreceptor structures are relatively preserved. In the outer nuclear layer (ONL), the number of nuclei is preserved. (C) 6 h after MNU injection, the inner segment of the photoreceptor (IS) is disorganised but the shortening and disorganisation of the outer segment of the photoreceptor (OS) is not obvious. In the ONL, the number of nuclei is preserved. (D) 24 h after MNU injection, the IS and OS are totally destroyed. In the ONL, the number of nuclei is decreased. (E) Magnified histology 6 h after the MNU injection. The outer nuclei in MNU injected rats are stained as well as in control retinas. The shortening and disorganisation of the IS can be observed; however, the OS is somewhat preserved 6 h after the MNU injection. (F) Magnified histology 24 h after the MNU injection. The shortening and disorganisation of the IS and OS are recognised. Chromatin of a small amount of outer nuclei is clumped.

Br J Ophthalmol 2011;**95**:1161–1165. doi:10.1136/bjo.2010.198317

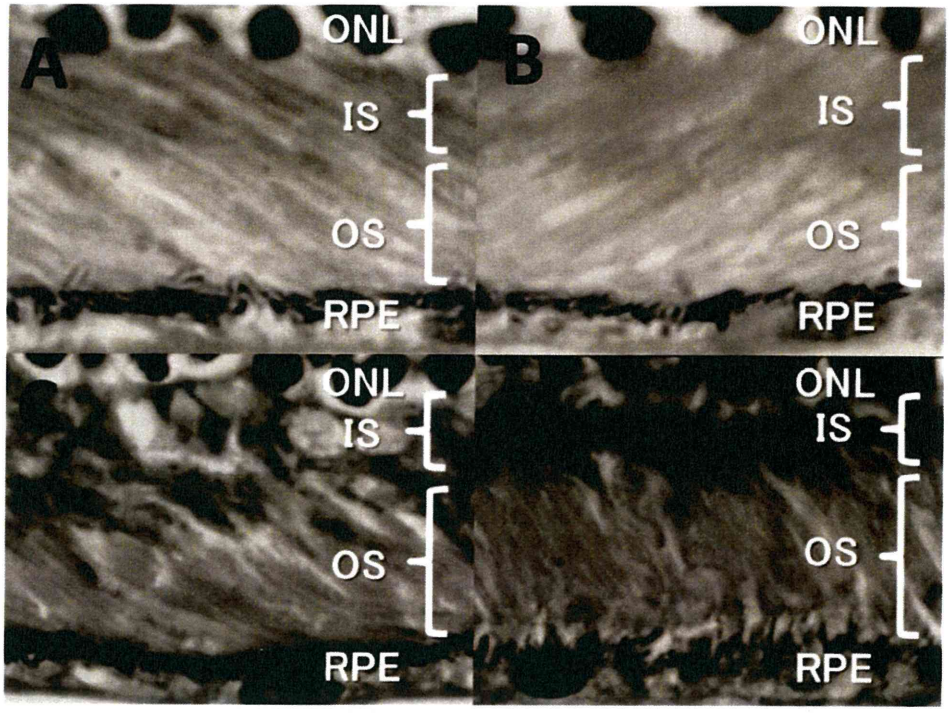

Figure 3 Magnified histology (magnification unknown) of the photoreceptor 3 h and 6 h after the *N*-methyl-*N*-nitrosourea (MNU) injection. (A, B) The structures of the inner segment of the photoreceptor (IS) and the outer segment of the photoreceptor (OS) are relatively preserved 3 h after the *N*-methyl-*N*-nitrosourea (MNU) injection, and the borderlines of the OS and IS are still recognised. (C) The IS is disorganised; however, the shortening and disorganisation of the OS are not obvious 6 h after the MNU injection. (D) The shortening and disorganisation of the IS is recognised; however, the OS is somewhat preserved 6 h after the MNU injection. RPE, retinal pigment epithelium.

somewhat preserved. The number of outer nuclei was preserved. The outer nuclei in MNU injected rats were stained as well as in control retinas. (figures 2C,E, 3C,D). Twenty-four hours after the injections, both the IS and OS structures had been totally destroyed, and the borderline between the IS and OS was indistinguishable. In the outer nuclear layer, the number of nuclei was decreased. Chromatin in a small amount of outer nuclei was clumped (figure 2D,F). One week after the injections, the photoreceptor cells disappeared, and several layers of cells remained between inner nuclei layer and choroid.

OCT images

In OCT images of the control retinas, the IS/OS were clear, straight lines that correctly represented the histopathology (figure 4A). In the OCT images of retinas obtained from rats 3 h after injection, the IS/OS also agreed with the histopathological

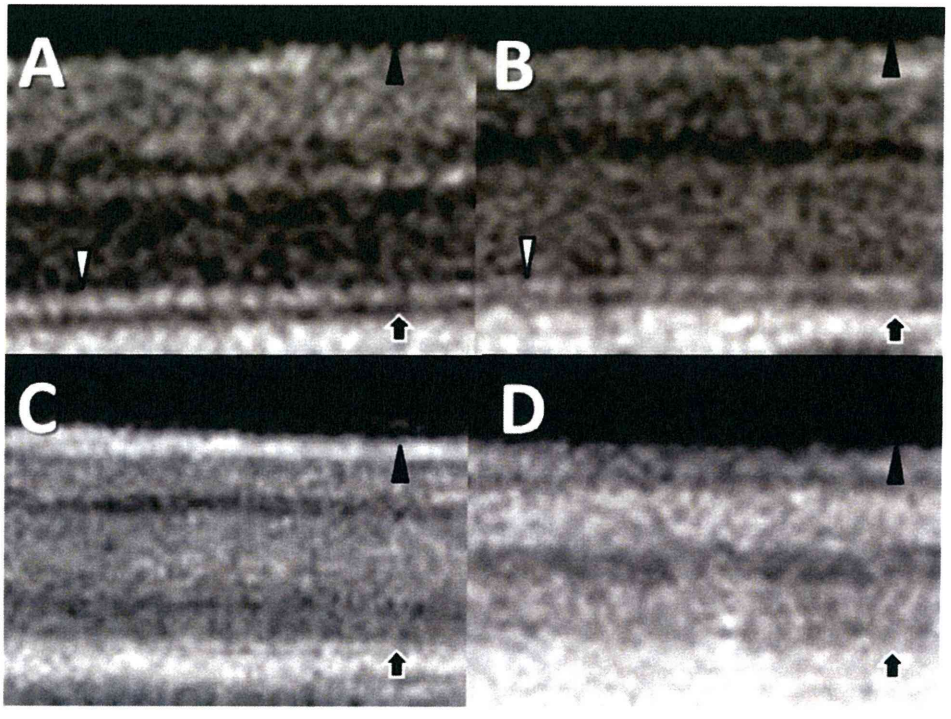

Figure 4 Optical coherence tomography images of retinas of control rats and rats injected with *N*-methyl-*N*-nitrosourea (MNU). (A) In a normal rat (corresponding to figure 2A), the intersection of the inner and outer photoreceptor segments (IS/OS) can be seen as a clear, straight line (white arrowhead). The arrow and black arrowhead shows the retinal pigment epithelium (RPE) line and internal limiting membrane (ILM) line, respectively. However, neither the external outer limiting membrane nor the intermediate line can be observed. (B) Three hours after the MNU injection (corresponding to figure 2B), the IS/OS can be seen as a relatively clear, straight line (white arrowhead). The arrow and black arrowhead show the RPE line and ILM line, respectively. (C) 6 h after the MNU injection (corresponding to figure 2C), the IS/OS is not observed. The arrow and black arrowhead show the RPE line and ILM line, respectively. (D) 24 h after the MNU injection (corresponding to figure 2D), the IS/OS is not observed. The arrow and black arrowhead show the RPE line and ILM line, respectively.